Modeling the relationship between stable isotopes in precipitation and mountain elevation

Beata Fiszer

Advisor: Mark Brandon
Second Reader: Ronald Smith

Wednesday April 30, 2014

A Senior Thesis presented to the faculty of the Department of Geology and Geophysics, Yale University, in partial fulfillment of the Bachelor's Degree.

Abstract

Mountains have a significant effect on the regional distributions of precipitation, producing high amounts of precipitation on windward slopes and low amounts of precipitation on leeward slopes. As an air mass is orographically forced upward, it systematically loses water vapor, preferentially raining out the heavier isotopes, H^2 (D) and O^{18}. This isotopic fractionation results in isotopic values becoming more negative at increasing levels of elevation. The strong correlation between isotopes in precipitation and elevation has led to a strong interest in the use of stable isotopes for quantitative measurements of paleoelevation. While various empirical estimates exist between modern elevations and corresponding isotopic values of precipitation, this study takes a theoretical approach. The linear theory of orographic precipitation (LTOP) developed by Smith and Barstad (2004) provides a solution for orographically forced precipitation given seven unknown atmospheric parameters. In this study, we use a modified version of LTOP to develop a model that estimates stable isotopic values given modern elevation data. Furthermore, we examine for the point at which isotopic fractionation occurs by comparing two cases, a condensation-equilibrated (CE) case and a precipitation-equilibrated (PE) case. Using 169 existing sample data points from the Patagonian Andes, we find values for eight unknown parameters that result in the best-fit relationship between estimated isotope values and observed sample isotope values. Results from our model support a PE case for fractionation, which agrees with previous estimates of fractionation occurring at 1 to 2 km above sea level. Moreover, for the best-fit condition, the model estimates 61.1% of the variance for δD and 48.1% of the variance for $\delta^{18}O$, supporting the continuation of development of this model for future work in elevation estimates.

Contents

1. Introduction

While numerous studies have found qualitative measurements of the paleoelevation of mountains, due to the difficulty in setting appropriate parameters and finding reliable methods, studies on quantitative paleoelevation measurements have only arisen in the last few decades. Quantitative measurements of paleoelevation are of great interest to scientists because elevation provides constraints on geodynamic processes happening in mountain belts (Rowley & Garzione 2007), influences biological events such as speciation, and has an impact on global and regional climate. Methods that have been developed include basalt vesicularity (Sahagian & Maus 1994), paleobotany (Forest & al. 1999) and a stable isotopes approach (Poage & Chamberlain 2001). Stable isotope-based analysis has been used for both empirical and theoretical estimates of paleoelevation (Rowley & Garzione 2007), and is a promising approach for further paleoaltimetry studies.

The stable-isotope based approach relies on the fractionation of H and 0 isotopes in orographic precipitation. As an air mass is forced to ascend up a mountain slope, it experiences adiabatic expansion and cools. Air becomes saturated with water vapor faster at cooler temperatures, causing the water vapor to condense as it rises (Rowley & Garzione 2007). The heavier isotopes of water, ^{18}O and D fall out first because they form stronger bonds and preferentially move into the lower energy level, the liquid phase. With increasing altitude, the air mass becomes depleted in ^{18}O and D resulting in more negative isotope ratio values in precipitation and surface waters (Poage & Chamberlain 2001). This effect has been described using the one-dimensional Rayleigh distillation model where α is the equilibrium fractionation factor which can be expressed for oxygen by the equation,

$$\alpha_O = R_p/R_v = (\delta^{18}O_p + 1000)/(\delta^{18}O_v + 1000). \quad (1)$$

R_p represents the ratio of ^{18}O/^{16}O in precipitation while R_v represents that ratio in water vapor. The same relation can be used for D/H fractionation (Rowley & Garzione 2007).

This relation has been used to establish an empirical relationship between elevation and isotopic lapse rates of δ^{18}O in precipitation and surface waters. Poage and Chamberlain found that in regions around the world other than those with extreme latitudes, the modern isotopic lapse rate is approximately .28ppm/100m (2001). While

this relationship gives a simplified version of orographic fractionation, it does not incorporate all the complexity that is involved (Risi & al. 2008). A linear theory of orographic precipitation that captures airflow dynamics, condensed water advection, and downslope evaporation was developed by Smith and Barstad (2004). The model presents a solution for the precipitation field of a complex region using eight unknown parameters: elevation, average wind speed, wind direction, initial isotopic composition of water vapor, temperature at sea level, humidity at sea level, lag time for condensation and fallout, and the moist Brunt-Väisälä frequency which measures the atmosphere's resistance to lifting (Smith & Barstad 2004). In 2007, Smith and Evans applied the model to stream water samples at varying elevations in the Patagonian Andes to test the model against real data. They found that their data created a good agreement between estimated isotope values and observed isotope values, but did not agree with previous samples taken by Stern and Blisniuk (2002).

This study uses a modified version of LTOP to model the relationship between stable isotopes from precipitation and mountain elevation. Three main questions will be addressed in this thesis. The LTOP model assumes a constant precipitation field for a region, although seasonality and natural variances such as storms have an effect on real terrain. We will examine whether we can find a mean precipitation rate that accurately represents the actual intermittent precipitation rate. Furthermore, water vapor and condensates are thought to be in quasi-equilibrium with the ability to continuously exchange isotopically. Therefore, we investigate where isotopes get set during the process. The two-end member cases are a condensation-equilibrated (CE) case and a precipitation-equilibrated (PE) case. The CE case assumes fractionation occurs when condensates form while the PE case assumes fractionation occurs when hydrometeors form. The final question asked in this thesis is whether we can find a general solution for the Stern and Blisniuk (2002) and Smith and Evans (2007) stable isotope data from the Patagonian Andes.

2. Model Formulations

2.1 Model Qualities and Parameters

A common simple method for estimating the distribution of precipitation in complex regions relies on estimates from the upslope model that uses regional slope and wind speed to determine the condensation rate above the terrain (Smith 1979). Even models that include advection of hydrometeors have several limitations in their application to real terrain. They assume instantaneous fallout of condensed water, constant orographically forced vertical velocity, and precipitation as only influenced by upslope regions (Smith and Barstad 2004).

Smith and Barstad's LTOP model addresses these assumptions and provides a method for determining a precipitation field for real complex terrain. It determines eight unknown parameters that describe the local atmospheric conditions of the region: average wind speed, wind direction, humidity and temperature at sea-level, the isotopic value of the initial vapor source, the hydrostatic stability of the atmosphere or the moist Brunt-Väisälä frequency, and delay times for formation of condensates and the fallout of hydrometeors (Smith and Barstad 2004). The delay times for condensation and fallout, T_c and T_F respectively, have been estimated to range from values of 200 to 2000s (Jiang and Smith 2003) and address the upslope-advection assumption of instantaneous fallout. Furthermore, mountain wave theory states that the vertical wind velocity of an air mass experiencing forced ascent will oscillate or decay depending on the stability of the atmosphere, the width of the mountain along the wind path, and the wind speed. The LTOP model is solved using the Fourier Transform to bring the variables into the wave domain. By solving for a vertical wavenumber and using the moist Brunt-Väisälä frequency, the stability of the atmosphere and its effect on air flow such as upwind tilting can be accounted for (Smith and Barstad 2004). The final solution in the LTOP model accounts for airflow dynamics, cloud delays and advection,

$$\hat{P}(k) = \left[\left(\frac{\rho_{s0}\Gamma_m}{\gamma}\right)\left(\frac{iuk}{(1-imH_w)(1+iuk\tau_c)(1+iuk\tau_f)}\right)\right]\hat{h}(k), \qquad (2)$$

where P(k) is the precipitation field, υ is wind speed, Γ_m is the moist adiabatic lapse rate, γ is the environmental lapse rate, h(k) is topography, H_w is the depth of the moist layer, m is the vertical wave number, and k is the intrinsic frequency.

Working off of the theoretical approach for the distribution of precipitation from the Smith and Barstad LTOP model, Dave Auerbach, Mark Brandon and I created a MATLAB program that relates stable isotope values to modern elevation given real data. Specifically, our model takes in real sample elevation data and given values for the eight unknown parameters, estimates isotope values for the sample locations. We test our model against the two previous studies (Stern and Blisniuk 2002; Smith and Evans 2007) to compare against the estimated stable isotope values. Comparing the model-estimated and observed sample isotope values and using climate dynamic data in the Patagonian Andes from previous studies (Garreaud 2013; Stern and Blisniuk 2002; Smith and Evans 2007), we find the best-fit parameters for our model.

Our model differs in its treatments of the available water vapor term, ρ_{s0}, by allowing it to vary along the trajectory path of the air mass, accounting for the reduced water vapor flux caused by lower amounts of water vapor available as it falls out as precipitation. While Smith and Evans addressed this issue by making local precipitation proportional to the local water vapor (2007), we make local condensation proportional to local water vapor. This adjustment accounts for local precipitation being advected from the original site of condensation.

Furthermore, studies vary in their interpretation of the point at which isotopes are set. The Rayleigh distillation model assumes that no isotope exchange occurs between cloud droplets and water vapor and that isotopes are set closer to the time of condensate formation (Stern and Blisniuk 2002). Another approach is that isotopes are set at cloud base about 1 to 2 km above sea-level, assuming that fractionation occurs closer to the time of hydrometeor formation. In order to examine where fractionation occurs in the atmosphere, we analyze two end-member cases, a condensation-equilibrated (CE) and a precipitation-equilibrated (PE) case. Our model calculates the estimated temperature for the formation of condensates and hydrometeors which is then used when estimating the isotope values. We then compare the isotope values estimated using the two cases against the sample isotope data and interpret the results.

Similar to the original LTOP model, our model takes in atmospheric data assuming certain uniform and constant parameters. While the parameters can be manipulated for

each trial, the wind speed, wind direction, moist stability of the atmosphere (N_m), and delay times are taken to be constant throughout each trial.

The moist Brunt-Väisälä frequency, N_m, is given by (Durran and Klemp 1982)

$$N_m \approx \sqrt{\frac{g}{T}(\Gamma_m + \gamma)}, \qquad (3)$$

where T is absolute temperature, Γ_m is the moist adiabatic lapse rate, γ is the observed lapse rate, and g is gravitational acceleration. The value of N_m also relates to the non-dimensional mountain height,

$$H_n = \frac{N_m h_{max}}{U}, \qquad (4)$$

where h_{max} is the maximum elevation of the mountain and U is the wind speed perpendicular to the mountain slope. When $H_n < 1$, the atmosphere is said to be unstable allowing an air mass to pass freely over the topography with constant wind velocity. As H_n approaches 1, the atmosphere becomes more stable and resistant to flow, a process referred to as blocking. Blocking occurs in mountains with relatively high topography, or areas of low wind speed causing the air mass to stagnate along its path, flow backward or flow around the mountain (Galewsky 2009).

2.2 Calculating the Vertical Wind Speed

The topography of a given mountain region is represented as h(x,y) and when $H_n < 1$, an unstable atmosphere, forced uplift mainly affects the vertical velocity of the air mass. The vertical velocity field, w(x,y,z) is the velocity of an air parcel that is forced vertically upward. The velocity field is solved following linear Boussinesq mountain wave theory (Smith 1979), with the result being calculated in the wave domain. The Fourier transform is applied to h(x,y) and w(x,y,z) to obtain their wave counterparts h(k,l) and w(k,l,z). MATLAB has a built-in function called the fast Fourier transformation (fft2) and its inverse (ifft2) that takes advantage of symmetric properties of complex roots and acts on the data in terms of periodicity (Shatkay 1995). The solution for vertical velocity in the wave domain is given as,

$$w(k,l,z) = i\sigma e^{imz} h(k,l), \qquad (5)$$

where the intrinsic frequency (rad/s) σ = ku + lv, $i = \sqrt{-1}$, and h(k,l) is the mountain wave transform of the topography h(x,y). Although, the equation accounts for the effects of topography on air flow, its scale is ignored so z can be thought of as zero (Smith and Barstad 2004). The vertical wave number is given as,

$$m(k,l) = \sqrt{(k^2 + l^2)[\frac{4\pi^2 N_m^2}{\sigma^2 - f^2} - 1]}\,, \qquad (6)$$

where f is the Coriolis frequency (rad/s). It is solved for with

$$f = 2 * 7.2921x10^{-5}\sin(latitude). \qquad (7)$$

Smith and Barstad determined that for mountains with horizontal scales between 100 m and 100 km, the Coriolis force can be neglected (2004).

Smith and Barstad simplified the equation to include only the k wave domain component reducing $m(k,l)$ to $m(k)$ (2004). This assumes a two-dimensional hydrostatic atmosphere. In our model, we keep the original flow path equation, to account for flow affected by topography along and across its path. Crapper found that vertical wind speed has horizontal components caused by diverted air from the trajectory path so we keep m in three dimensions (1959).

In the initial trials of the model, N_m ranged from .0005 s^{-1} to .01 s^{-1} but remained uniform throughout the given trial. The σ^2 was determined by the wind speed given to the model and by a program that calculated the intrinsic frequency values on a point on the given flow path. Thus, the σ^2 changed for each point during the given trial.

The vertical wave number is influenced by the relationship between σ^2 and N_m^2, so the wind speed and Brunt-Väisälä frequency have a strong effect. For instance, if $\sigma^2 > N_m^2$, (6) reduces to $m = \sqrt{4\pi^2 i(k^2 + l^2)}$, m becomes positive imaginary, and the forced air mass decays as it moves upward. If $\sigma^2 = N_m^2$, m becomes zero and the forced waves will rise in phase, but will not decay. If $\sigma^2 < N_m^2$, m becomes real signifying a stable atmosphere in which the forced waves propagate upstream. In this case, the air piles up on the windward side of the mountain, and the isotopic signal of the orographic precipitation may appear lighter (Nappo 2002).

2.3 Calculating the Precipitation Field

The precipitation field is calculated using the version of the linear theory of orographic precipitation developed by Smith and Barstad (2004) and modified by Mark Brandon. At sea level (h=0), ρ_{s0} is solved by

$$\rho_{s0} = \frac{e_s(T_0)}{R_v T_0}\ , \qquad (8)$$

Where e_s is the partial pressure of water vapor, T_0 is temperature (K) at sea level, and R_v = 461 J $kg^{-1}K^{-1}$ and represents the partial law constant for water vapor. The value for ρ_s decreases with increasing elevation and is proportional to e^{-z/H_w}. In our calculations, water density is defined by

$$\rho_s(x,y,z) = \rho_{sr}(x,y)e^{-z/H_w}. \qquad (9)$$

The density for initial water vapor available, ρ_{s0}, is treated differently in our model than in the earlier Smith and Barstad and Smith and Evans versions. It varies spatially along the flow path and accounts for changes in the water vapor flux caused by precipitation of a lifting air mass. In the original LTOP model (2004), the water vapor flux was taken to be proportional to the flux at the original vapor source. The flux is in fact reduced as the air mass loses the available water vapor along its path, so this approach can overestimate the amount of precipitation occurring at a given elevation. Smith and Evans improved this characteristic by making the water vapor flux proportional to the local precipitation rate (2007). This approach provides a better estimate for the flux at a given elevation, but it does not account for local precipitation being advected from the point of condensation. In our model, we make the water vapor flux proportional to the local condensation based on modifications calculated by Brandon.

The source rate, represented by S(x,y), is the initial condition at which water is produced. Source rate depends on vertical wind speed, w(x,y,z), and performing vertical integration as it is orographically lifted gives the relationship,

$$S(x,y) = \frac{\rho_{sr}(x,y)\Gamma_m}{\gamma H_w}\int_0^\infty w(x,y,z)e^{-z/H_w}dz. \qquad (10)$$

The $\rho_{sr}(x,y)$ term can be estimated with the introduction of a relative variable for source rate,

$$\hat{r}_s(k,l) = \frac{S(x,y)}{\rho_{sr}(x,y)} = \frac{\Gamma_m}{\gamma H_w}\int_0^\infty w(x,y,z)e^{-z/H_w}dz, \quad (11)$$

which is in the wave domain and can be solved by using the Fourier Transform. The only variable that varies in the horizontal is the vertical wind speed, and it can be transformed into the wave domain by combining (5) and (11), which gives

$$\hat{r}_s(k,l) = \left[\left(\frac{\Gamma_m}{\gamma}\right)\frac{i\sigma}{1-imH_w}\right]\hat{h}(k,l). \quad (12)$$

Incorporating the solution of $\hat{r}_s(k,l)$, the relative precipitation rate can be found by adding the time-delay equations for condensation and fallout using the LTOP equation,

$$\hat{r}_p(k,l) = \left[\left(\frac{r_m}{\gamma}\right)\left(\frac{i\sigma}{(1-imH_w)(1+i\sigma\tau_c)(1+i\sigma\tau_f)}\right)\right]\hat{h}(k,l). \quad (13)$$

The absolute precipitation rate is found by taking the maximum value of (13),

$$P(x,y) = \max[r_p(x,y),0]\rho_{sr}(x,y), \quad (14)$$

where the max function ensures positive precipitation (Smith & Barstad 2004).

Smith and Evans accounted for the change in available water vapor by making the local water vapor flux (F(x,y)) proportional to the local precipitation (P(x,y)). The local water vapor flux can be represented by

$$F(x,y) = \rho_{sr}(x,y)H_wU. \quad (15)$$

The H_w and U terms are spatially uniform while ρ_{sr} varies in space which accounts for the decrease in water vapor available as the air experiences orographic precipitation.

In order to solve for p_{sr}, we integrate back along the path (s) in the given wind direction. The local precipitation rate is now determined by P(s) where s=0 represents the local region of interest and increases in the downwind direction. Differentiating (15) gives

$$\frac{dF(s)}{ds} = H_wU\frac{d\rho_{sr}(s)}{ds}. \quad (16)$$

Substituting s for the coordinates in (15) we get,

$$P(s) = -\frac{dF(s)}{ds} = r_p \rho_{sr}(s). \qquad (17)$$

Combing (16) and (17) results in

$$\frac{d\rho_{sr}(s)}{\rho_{sr}(s)} = -\frac{r_p(s)}{H_w U} ds, \qquad (18)$$

Which when integrated provides the change in water vapor density along the wind path (s) where s = -∞ equals the initial upstream value,

$$\rho_{sr}(s) = \rho_{s0} \exp[-\frac{1}{H_w U} \int_{-\infty}^{s} r_p(s') ds']. \qquad (19)$$

The final water vapor density is represented by $\rho_{s0}(k,l)$ in the wave domain. This approach provides the most accurate solution for the resulting precipitation field and is used to solve for the maximum precipitation rate (14).

2.4 Estimating Stable Isotopic Values

As mentioned earlier, during orographic precipitation, a lifting air mass becomes isotopically lighter as the heavier isotopes of precipitation preferentially fallout. In the case of Rayleigh distillation, fractionation is set closer to the formation of hydrometeors (Stern & Blisniuk 2002). This process is due to a constant exchange of molecules between the water vapor and the hydrometeors until fallout of the hydrometeors occurs. Another case assumes that fractionation occurs closer to formation of condensates. This approach could be more plausible for ice because it exchanges more slowly with water vapor than with water (Rowley 2002). In order to test the validity of these two approaches we establish two end member cases, a condensate-equilibrated case (CE) and a precipitation-equilibrated case (PE). The CE case represents the case in which isotopes are set at the formation of condensation while the PE case represents the case in which isotopes are set at the formation of hydrometeors. The limiting temperatures for equilibration are calculated for each case and compared in our model. For the CE case, the temperature for the source, T_p, is used while for the PE case, the land surface temperature, T_s, is used. Our model assumes the atmosphere is saturated vertically, so the isotopic composition of the hydrometeors in the latter case is set close to land surface temperature.

The equations for the two limiting temperatures are solved for as follows,

$$T_p(x,y) = T_0 - \Gamma(h(x,y) + z_p(x,y)), \quad (20)$$

$$T_s(x,y) = T_0 - \Gamma h(x,y), \quad (21)$$

where z_p is the mean height of precipitation given by,

$$z_p(x,y) = \int_0^\infty z r_p(x,y,z)dz \,/\, \int_0^\infty r_p(x,y,z)dz. \quad (22)$$

The isotopic composition is solved for both of these cases using the Rayleigh fractionation equation (1). More general forms for the mass ratios of stable isotopes in the vapor and hydrometeor are given as follows, respectively,

$$\frac{dR_v}{R_v} = (\propto(T) - 1)\frac{dF}{F}, \quad (23)$$

$$R_p = \propto(T) R_{v.} \quad (24)$$

F represents the water-vapor flux, and α is the temperature-dependent fractionation factor. The fractionation factor is solved for differently depending on whether it is in the ice or water state. The final solutions for the isotopic values of oxygen and hydrogen are solved for using experimentally determined relationships by Horita and Wesolowski (1994) and Ellehoj & al (2013). The outputs of the model give samples in standard delta notation,

$$\delta = \frac{R_{sample}}{R_{standard}} - 1, \quad (25)$$

The final solution for the isotopic composition of precipitation at a given sample is given by,

$$\delta_p(s) = \ln\left[\frac{\alpha(s)}{\alpha(-\infty)}\right] + \delta_p(-\infty) - \frac{1}{H_w U}\int_{-\infty}^{S}(\propto(s') - 1) r_p(s')ds', \quad (26)$$

where the variable s represents the flow direction.

3. Application of the model to the Patagonian Andes

3.1 Study Region

The study site is located in the Patagonian Andes, a diverse mountain range divided into Chile on the West and Argentina on the East. The Patagonian Andes lie in a region where the wind is predominantly westerly due to the Coriolis effect that is caused by Earth's

rotation. This region is a strong example of the rain shadow effect with up to 6000 mm of rain fall per year on the windward side of the mountain while only 300 mm fall per year on the leeward side (Smith & Evans 2007). The western coast extends out to the Pacific Ocean, the main water source for the precipitation falling on the mountain, which avoids possible complications that could arise from mixed water sources. Furthermore, the modern elevation reaches around 2000 m, which is high enough to have a significant effect on uplift, but not too high to cause blocking or wind divergence around the mountain (Stern & Blisniuk 2002). This region is a straightforward example of orographic precipitation and has been studied greatly for is orographic effects.

Smith and Evans collected 71 stream samples in the Patagonian Andes between 40°S and 47°S recording $\delta^{18}O$ values, δD values, and elevation (2007). These samples used LTOP and found a best-fit relationship between their model results and the observed results with a co-efficient of efficiency of 0.530 for deuterium. However, they were unable to find a good-fit between their data and that of Stern and Blisniuk collected between 47°S and 48°S (2002). In this study, we combine all 169 sample points collected by the two studies and apply the modified LTOP to the analysis to find whether our model can produce a best-fit result that accounts for a good proportion of variance for all the data (Figure 1).

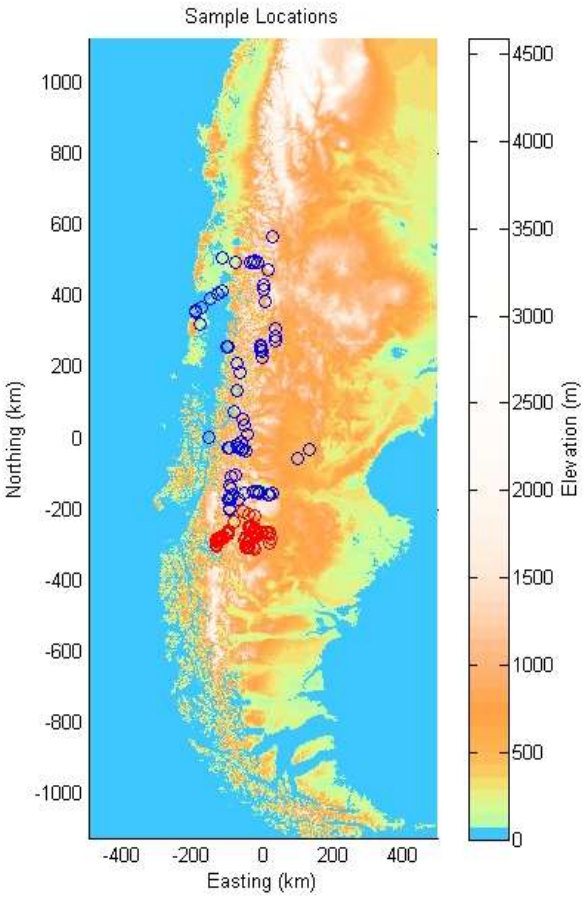

Figure 1 Stern and Blisniuk (red) and Smith and Evans (blue) samples presented on a topography field map of the Patagonian Andes.

3.2 Establishing Azimuth for Wind Direction

The wind speed hitting the mountain is taken to be independent of time and space, represented by the vector U = Ui + Vj (Smith & Barstad 2004). An estimate of wind directions of the Patagonian Andes was determined by Smith and Evans using NCEP-NCAR analysis from 2005 (Figure 1) (2007). Wind predominately came from the West remaining between 0 and 180 degrees.

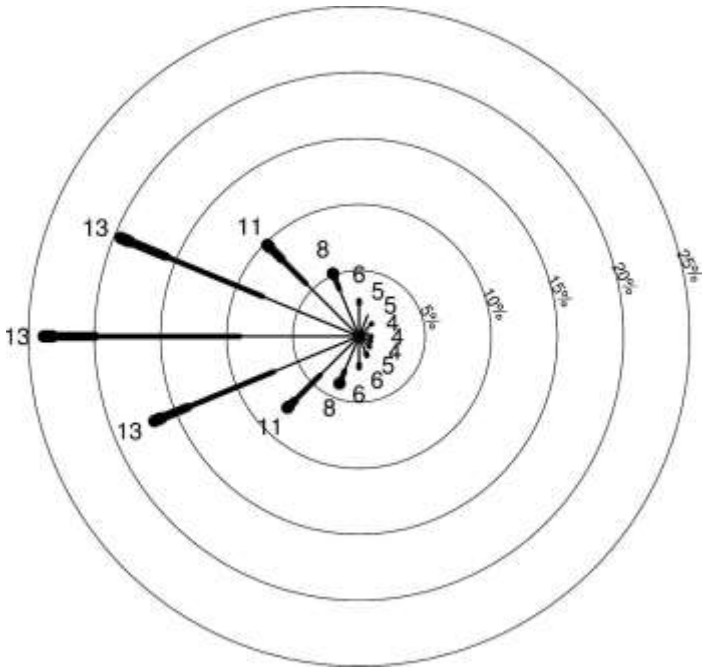

Figure 2: Coastal wind rose from the southern Andes where length of the radial line translates to frequency of wind direction and number refers to wind speed (m/s). Smith and Evans 2007

In order to incorporate the Patagonian Andes samples into our model, initial sample point locations were given as longitude and latitude points as separate data sets. We decided to create a grid with location in values of Northing and Easting with (0,0) located at the center of the 169 sample points. The padding of the grid box was chosen to be able to create a transect that started from the water source, the Pacific Ocean and went in the direction of an estimate of the maximum scope of westerly winds the Patagonian Andes receives.

The next step was to find a range of azimuth values that captured the maximum and minimum wind direction for the grid box. The goal was to find an upper and lower bound for wind trajectory lines that ran through each sample point entering through the western border and leaving through the eastern border of the grid box. Keeping wind direction within this range ensures that each trajectory line begins in the Pacific Ocean and thus uses the moisture source for its initial conditions.

We noted that the maximum and minimum directions could only be azimuths for a line that connected a sample point location to one of the four corners. Furthermore, each sample point only had one maximum and minimum azimuth value. In order to find these values for each sample point, the grid box was divided into quadrants (Figure 3).

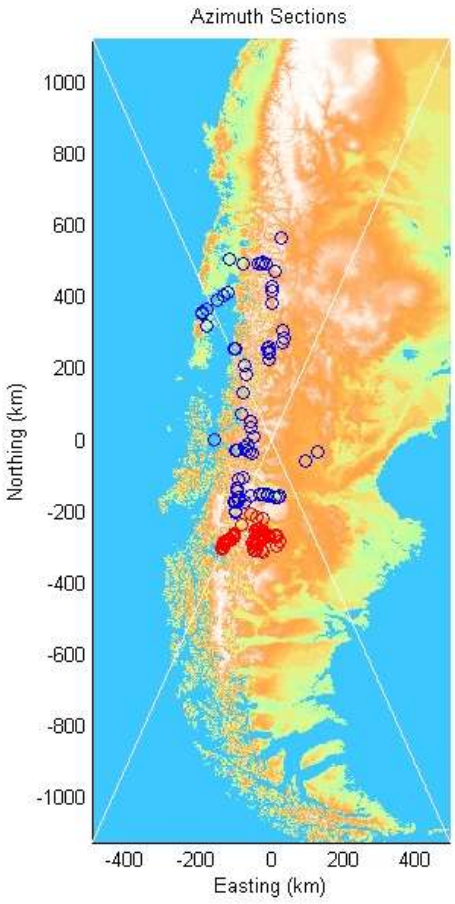

Figure 3 Azimuth sections labeled in counterclockwise order starting with the western quadrant as Quadrant A

A test was conducted comparing the azimuth values of the two lines dividing the grid box into quadrants and azimuths of a line from each sample point to the Northwest corner and a line from each sample point to the Southwest corner of the grid box. This placed each sample point into one of the quadrants. The minimum and maximum azimuth values for quadrants A through D are given as follows (Table 1):

Table 1 Lines for maximum and minimum azimuth through each sample point

Quadrant	Maximum Azimuth	Minimum Azimuth
A	(Sample, Northwest corner)	(Sample, Southwest corner)
B	(Southeast corner, Sample)	(Sample, Southwest corner)
C	(Southeast corner, Sample)	(Northeast corner, Sample)
D	(Sample, Northwest corner)	(Northeast corner, Sample)

The maximum and minimum azimuth was found by comparing the maximum and minimum azimuths of each sample point. This method is transferable to other grid locations and could be used to determine a range of wind directions for other orographic regions.

The initial calculation involved the range of azimuths appropriate for the possible wind direction for the Patagonian Andes. The resulting azimuth range was 45.0633° to 136.6426°, with azimuth set as 0° at North and 90° at East edge (Figure 4). This range is a conservative estimate of possible wind directions that are present in the Patagonian Andes region.

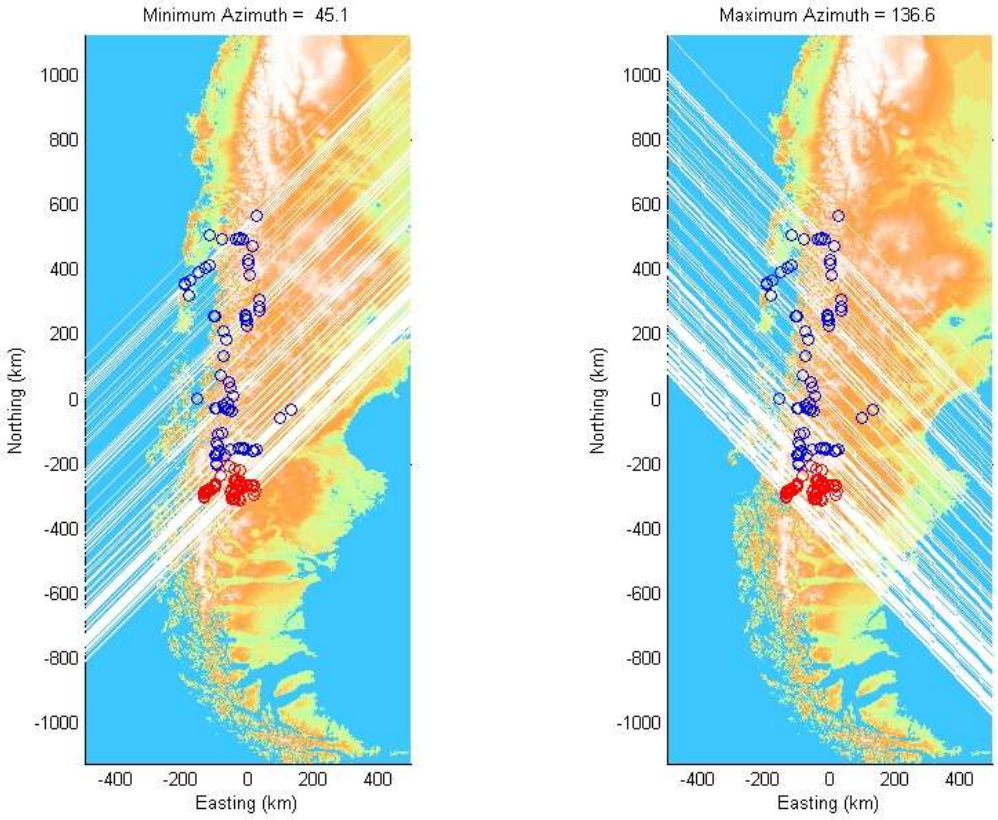

Figure 4 Wind paths through each sample point at the maximum and minimum azimuth values

The wind trajectory lines were then segmented into 1 km-grid spacing in order to be able to integrate back along the path in later calculations.

3.3 Finding the best-fit parameters

Inputting elevation data, h(x,y), from the Stern and Blisniuk (2002) and the Smith and Evans (2007) sample points, we were able to test 169 sample points. The Patagonian Andes region of study has a horizontal scale greater than 300 km, thus the Coriolis force was

included in the calculations. The latitude value which is used as input to find the effects of the Coriolis force was estimated as 45° based on the average latitude of the sample points. Using equation (7), the Coriolis frequency (f) for our trial runs was 1.03×10^{-4} rad/s. The initial isotope values were estimated as -52.8 ppm for D and -5.3 ppm for ^{18}O. The values for wind speed, wind direction, delay time, surface temperature and the moist Brunt-Väisälä frequency were initiated at the beginning of each run. An initial function calculated Γ_m, γ, H_w, and ρ_{s0} using sea surface temperature (T_0) and N_m.

The input parameters were tested for by comparing the sample isotope values at a given elevation to the isotope values estimated by the model. The values were compared by first calculating a standard deviation for each with

$$SD = (\delta R_S - \delta R_E)\sqrt{n/(n-8)}, \quad (27)$$

where δR_s is the sample isotope value, δR_E is the estimated isotope value, and n is the sum of samples. Note, the denominator of the square root is subtracted by 8 due to the number of unknown parameters used in the model. The lower the SD value, the better the model agrees with the observed data. Once the SD value was calculated, the R-squared relationship could be found with

$$R - squared = 1 - (SD/SD_{observed})^2, \quad (28)$$

where $SD_{observed}$ is equal to the standard deviation of the total observed isotope values, D = 21.50183 and ^{18}O = 2.731646. The greater the R-squared value, the better the variance of our model agreed with the natural variance of the sample data.

The model was run approximately 100 times to check for the best-fit parameters with differing input values for U, azimuth, τ_f and τ_c, T_0, and N_m. Each trial took approximately 45 seconds to complete when all figures were included. The values for U, azimuth and T_0 were estimated using PRECIS-DGF results from the year 1980-1990 for the Patagonian Andes region (Garreaud 2013). Smith provided limits for the horizontal wind components as 1-50m/s, N_m as $0.01s^{-1}$, and τ_f and τ_c as 200-2000s (2006). In the initial trails, azimuth = 125°, τ_f and τ_c = 800, T_0 = 280, and $N_m = 0.001s^{-1}$. Wind speed was varied between 5m/s and 50m/s. Next, the azimuth was changed between 90° and 135° following the upper

limit of the original azimuth limit for our model's location and a Northwesterly correlation between precipitation amount and wind direction developed by Garreaud (2013). Smith and Evans found that the values for τ do not experience drastic changes with altering values for fallout and condensation (2007). Rather, the sum of the τ values is important. The delay time values in the trials ranged from 600 s to 800 s. The value of T_0 ranged from 267K to 283K based on annual temperature values estimated using PRECIS=DGF data (Garreaud 2013). Estimates for N_m ranged from .0005 s^{-1} to .01 s^{-1} which has a lower bound than the original limit proposed by Smith for LTOP (2006). This range was determined based on an estimate of $N_m = 0.003\ s^{-1}$ for the Patagonian Andes by Smith and Barstad (2007).

In every trial, the δD and $\delta^{18}O$ for the CE and PE cases were estimated at each sample elevation. The CE case and PE case were distinguished by the use of either the T_p or T_s temperature, respectively to solve for the stable isotopes in each. The T_p temperature was estimated at the precipitation height solved by equation (22). The model solved for the temperature of each case on the model grid producing cooler source temperatures (T_p) and warmer surface temperatures (T_s), as expected (Figure 5).

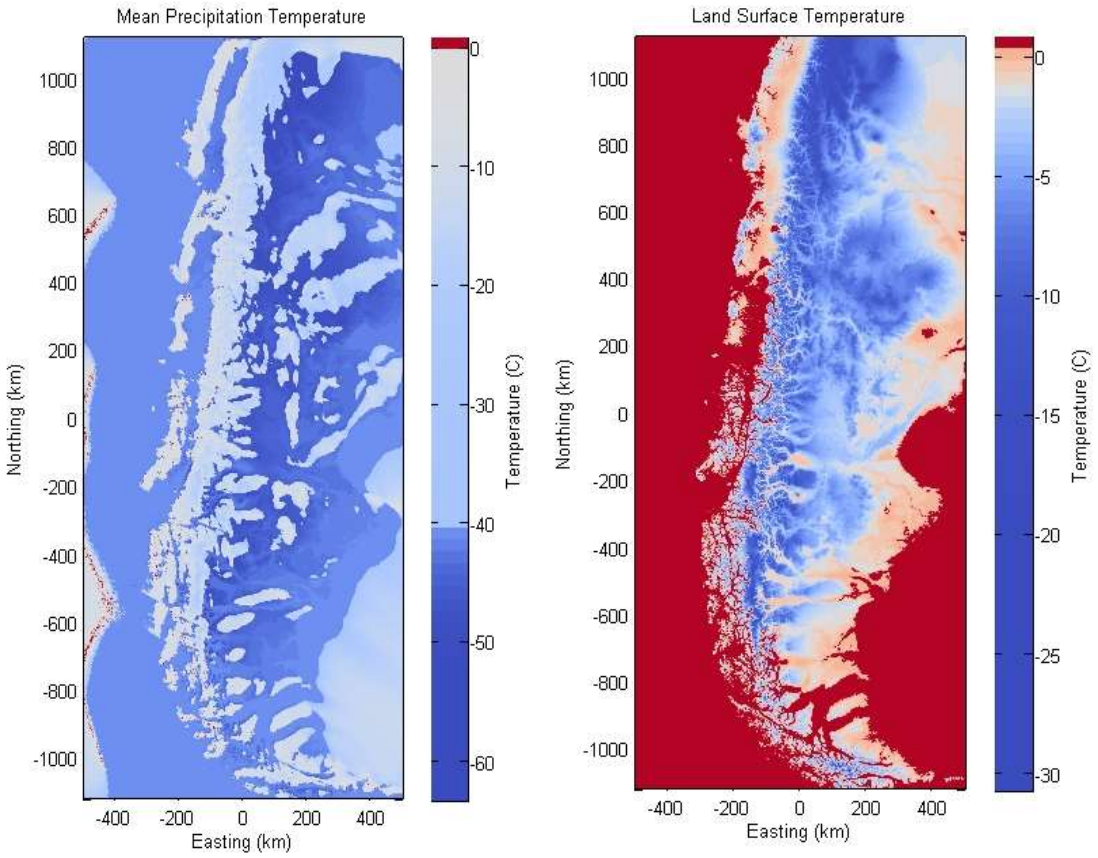

Figure 5 (Right) Mean precipitation temperature (T_p) for the CE case under best-fit parameters. (Left) Mean surface temperature (T_s) for PE case under best-fit parameters.

The model program returned an estimate for the scale height, H_w, regional mean precipitation height, and a standard deviation value for δD_{CE}, $\delta^{18}O_{CE}$, δD_{PE}, and $\delta^{18}O_{PE}$. The parameters for the best-fit solution support the PE case, while the CE case was unsuccessful in creating a meaningful agreement between the estimated and observed isotopic values (Figure 6).

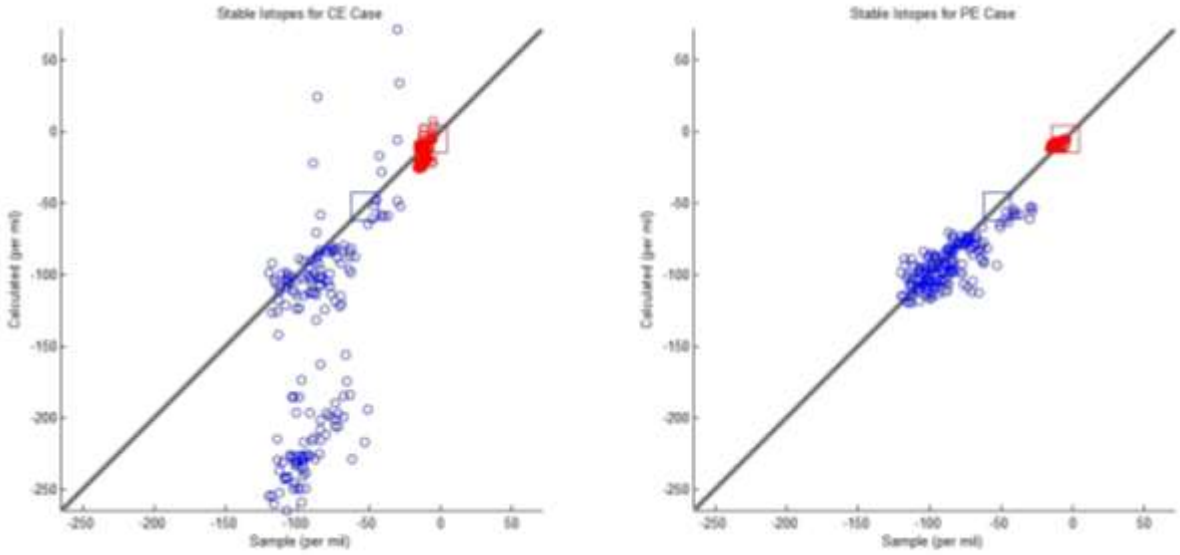

Figure 6 Comparison of the correlation between observed stable isotopes and estimated stable isotopes for the CE and PE cases. The parameters given represent the best-fit case. The blue represents δD values while the red represents $\delta^{18}O$ values.

The best-fit solution was determined by the R-squared value for δD_{PE} because it gave the best agreement to the model. All the trial runs produced negative R-squared values for the CE case, presenting no correlation between the model results and the observed results. The best-fit parameters for the model were a wind speed of 30 m/s, azimuth of 132°, τ_{total} of 1450 s, T_0 of 274 K, and N_m of 0.001 s^{-1}. Under these parameters, the model produced a linear fit of 61.1% for δD and 48.1% for $\delta^{18}O$ (Table 2).

Table 2 Sample trial runs for the model with Stern and Blisniuk (2002) and Smith and Evans (2007) Patagonian Andes sample data. The first values indicate the best-fit parameter case. The upper and lower range values for each value that was varied between trials is shown as well (bold). These trials were run with the Coriolis Frequency included.

U(m/s)	Azimuth(deg)	$\tau_F = \tau_C$(s)	T_0 (K)	$N_m(s^{-1})$	R^2 δD_{CE}	R^2 $\delta^{18}O_{CE}$	R^2 δD_{PE}	R^2 $\delta^{18}O_{PE}$
30	132	725	274	0.001	-8.21457	-4.46666	0.610702	0.480648
5	132	725	274	0.001	-8.17241	-5.05569	0.465179	0.326975
50	132	725	274	0.001	-4.92715	-2.58393	0.57558	0.438468
30	**90**	725	274	0.001	-5.33955	-2.92699	0.422675	0.286272
30	**135**	725	274	0.001	-7.24055	-3.91293	0.529095	0.439762
30	132	**600**	274	0.001	-8.61027	-4.62015	0.573676	0.475761
30	132	**800**	274	0.001	-7.93041	-4.32568	0.599973	0.464141
30	132	**0**	274	0.001	-92.9856	-54.4171	-43.9167	-28.3942
30	132	725	**267**	0.001	-8.4931	-4.5859	0.401515	0.42181
30	132	725	**280**	0.001	-8.4096	-4.59054	0.549355	0.426361
30	132	725	274	**0.0005**	-8.80569	-5.19936	0.577566	0.492655
30	132	725	274	**0.01**	-17.3297	-11.5549	-0.46966	-0.33058

Table 2 also shows the effects and trends of higher and lower values for each parameter. Due to the negative results for the CE case, only the PE case was analyzed for the effects of changes in the parameters on the R-squared values. Higher wind speeds resulted in a better fit than lower wind speeds. Wind directions from a Northwesterly direction fit better than those from a Westerly direction. The τ range in this model did not have a significant effect when changing from higher to lower values. However, values of 0 s did result in a bad-fit for both cases, supporting the importance of the delay times in the model. Higher temperature gave a better fit for $\delta D_{PE,}$ but did not experience a significant change for $\delta^{18}O_{PE}$ than lower temperatures (T_0 < freezing). The N_m values had a large effect on R-squared values, with a value of 0.01 s^{-1} resulting in negative values.

The model calculated a value of 2024 m for the scale height, H_w, and 1172 m for the mean precipitation height. The model also returned values for the vertical wind speed for an air mass at any given location on the grid map (Figure 6).

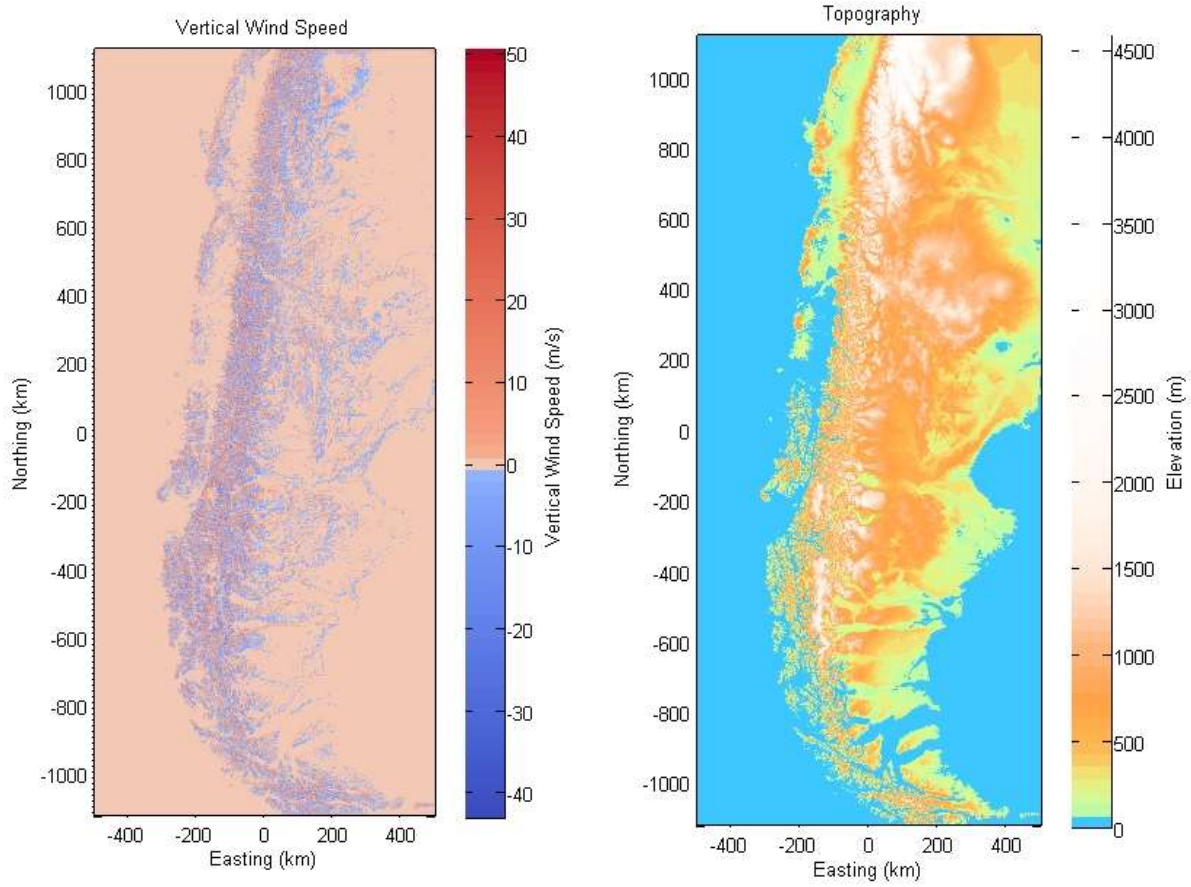

Figure 7 Vertical wind speed predicted by the model under best-fit parameter case in comparison to topography of the region.

The vertical wind speed ranges from approximately -40 m/s to 50 m/s. For an incoming speed of U = 30 m/s, values estimated for the vertical wind speed above do not agree with the notion that the wind speed will either stay constant or decay in its vertical component. The graph does show a majority of points falling within the 20 m/s to -10 m/s range.

One of the aims of the study was determining whether the model can accurately represent intermittent rain with a mean precipitation rate. The relative precipitation rate was calculated in proportion to the available water vapor at the location of precipitation (Figure 7).

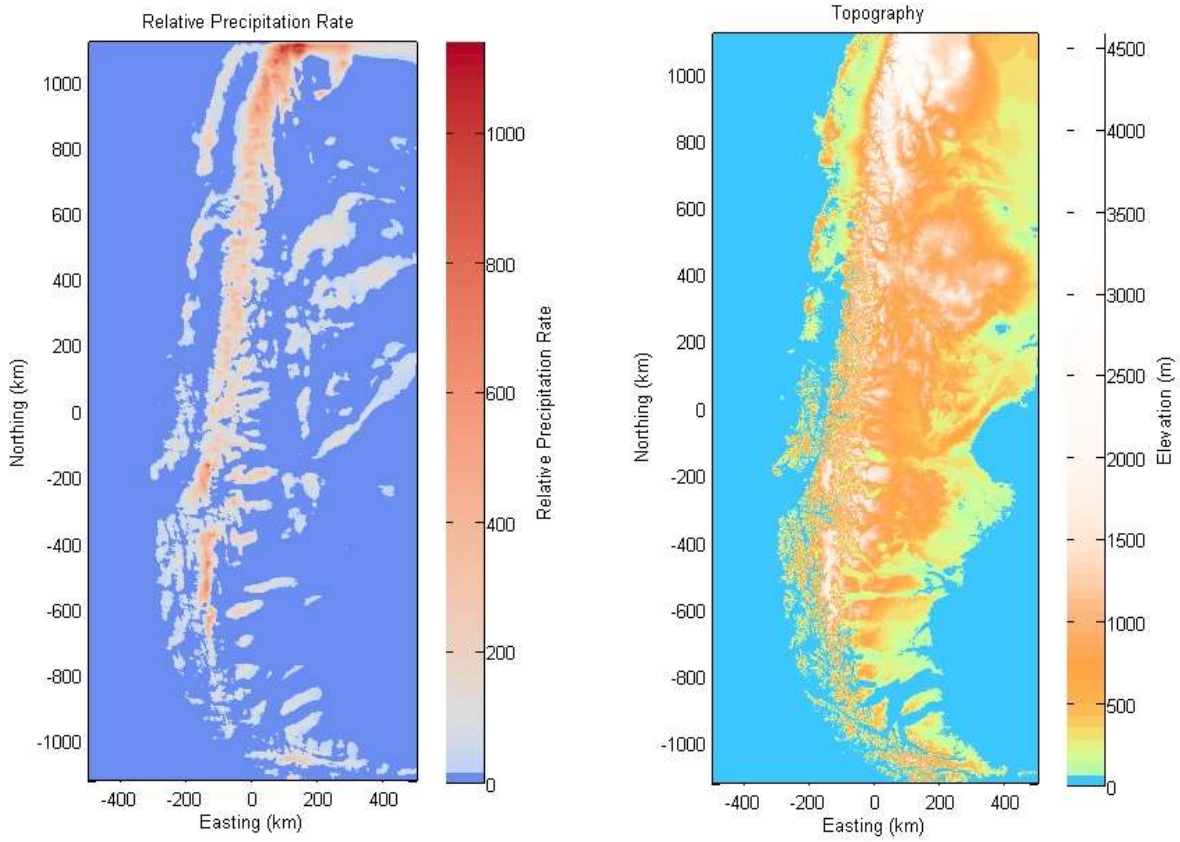

Figure 8 Relative precipitation rate predicted by the model under best-fit parameter case in comparison to topography of the region. The precipitation rate is relative to available water vapor at the given location.

The orographic precipitation effect is captured with the model with more precipitation falling on the windward side of the mountain as expected and less precipitation falling on the leeward side.

4. Discussion

This project sought to answer three main questions: whether the model could accurately represent the precipitation of a complex region with intermittent rain patterns, whether isotopes are set closer to the time of condensate formation or closer to the final formation of hydrometeors, and whether it could produce a common best-fit parameter for the Smith and Evans (2007) and Stern and Blisniuk (2002) sample sets.

The model does a good job of estimating the relative precipitation rate of the Patagonian Andes. This region has a strong and steady wind pattern that moves from West to East creating more precipitation on the Western side of the mountain and a rain shadow on the Eastern slopes. For the case of the Patagonian Andes, the model is able to reproduce the orographic effect seen in the region. As mentioned earlier, the Patagonian Andes are a simple case of atmospheric flow so the model may not be as effective in more complicated terrains. This result does show that even with intermittent rain and seasonality, the Patagonian Andes do have a mean precipitation rate that can represent the region for input in stable isotope calculations.

Furthermore, the results support a precipitation-equilibrated (PE) approach to isotopic fractionation. In this case, hydrometeors and water vapor are free to exchange during the formation of precipitation, and the isotopes do not get set until the fallout occurs. In our model, the air is vertically saturated during precipitation events meaning that the location of fallout is represented by the surface temperature. R-squared values for δD showed a better fit than R-squared values for $\delta^{18}O$. This may be due to noise in the oxygen data in the samples. Smith and Evans also found better agreement with the δD values than the $\delta^{18}O$ values (2007).

Our best-fit parameters were found by searching for the best fit, least variant result between the observed and estimated stable isotopes. The parameter results do agree with observable atmospheric conditions. The wind direction of 132° agreed well with the climate data presented by Garreaud (2013) (Figure 9).

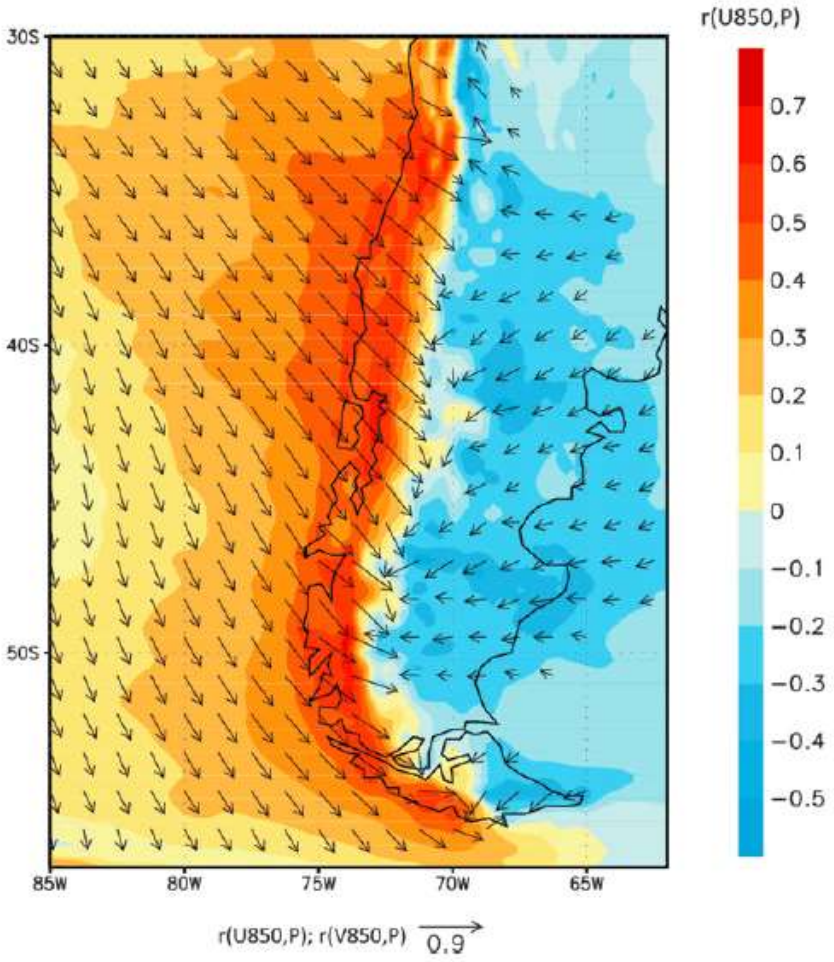

Figure 9 Correlation between precipitation and average wind direction during precipitation amounts. The area of interest is located between 40°S and 48°S with a precipitation wind direction coming from the Northwest.

The wind speed at 30m/s is much larger than the average wind speed found by Smith and Evans of 11m/s (2007). Their wind speed estimates were shown for average wind speed without a correlation with amount of precipitation. The higher wind speed presented by our model may imply that wind that forms precipitation over the Patagonian Andes moves with a higher magnitude. As mentioned earlier, wind speed also has an effect on the intrinsic frequency of an air mass experiencing forced uplift where $\sigma^2 < N_m^2$ creates a more stable atmosphere. The variable σ^2 is dependent on wind speed so a smaller wind speed would lead to a more stable atmosphere. Our results agree with an unstable atmosphere with a large magnitude for wind speed.

The stability of the atmosphere also depends on N_m. Our model estimates a value of 0.001 s^{-1} which is close to Smith and Evan's estimate of 0.003 s^{-1} (2007). Going back to the

relationship between σ^2 and N_m^2, when $N_m^2 < \sigma^2$, the atmosphere is assumed to be unstable. A large value of N_m at 0.01 s^{-1} led to negative values for R-squared. This trend also supports the claim that our model works for an unstable atmosphere and that an air mass is able to flow over the Patagonian Andes with limited blocking.

Smith and Evans found that a total delay time of 1700 s using the LTOP model for the Patagonian Andes fit well (2007). Our model estimates a total delay time of 1450 s. The range of values used for delay time in the trials did not result in significant changes in R-squared values so our value seems within range with the earlier Smith and Evans value. When delay time for condensation and fallout were initialized as 0 s (case of instantaneous fallout), the resulting R-squared values for the PE and CE cases were large negative numbers, implying a significance of delay time for our model.

The best-fit parameter for temperature, 274K, was found to be close to the freezing temperature of 273.15K. The PRECIS-DGF data for our sample location shows temperatures that fall between 0°C and 5°C or 273.15K and 278.15K (Garreaud 2013) (Figure 10).

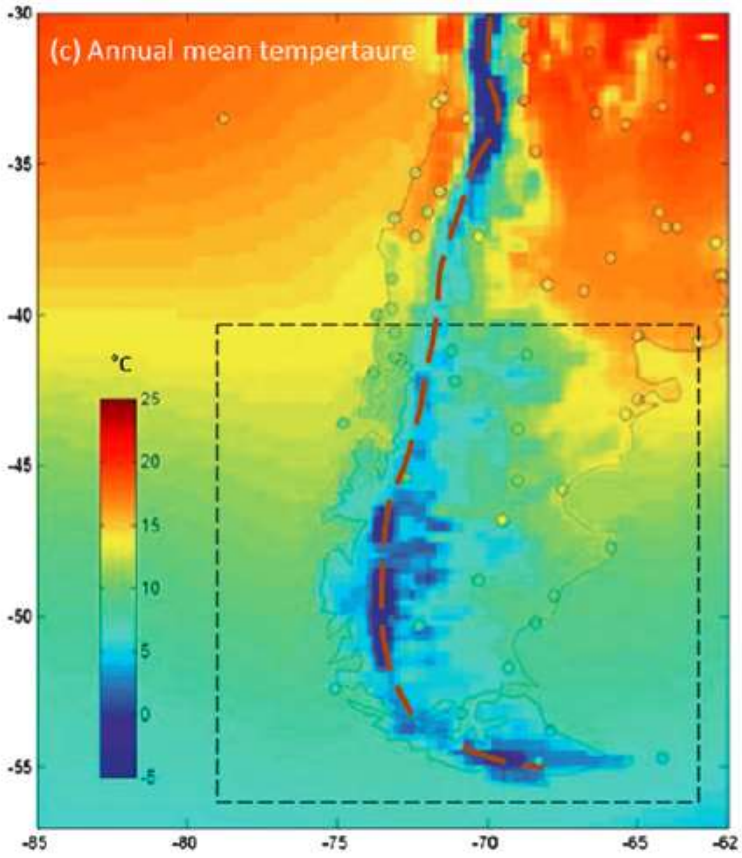

Figure 10 Garreaud 2013 PRECIS-DGF near surface temperature (shaded) compared against monthly data in station observations (circles) for the period 1978-2001.

The final question addressed whether the Smith and Evans data and the Stern and Blisniuk data for stable isotopes in the Patagonian Andes could be solved for with a model. Our model resulted in 61% agreement for δD and 48% for $\delta^{18}O$. An agreement of 100% in the R-squared value would mean that the model accounts for all the variance occurring in the natural terrain. The Patagonian Andes is a complex region with a lot of natural variance. The R-squared values we calculated under best-fit conditions show a promising ability for the model to estimate stable isotopes. These results show that we were able to model stable isotopes resulting from isotopic fractionation in precipitation for a complex region using mean climatic properties.

5. Summary

The climatology of the Patagonian Andes provides a straightforward setting to study the effects of orographic precipitation and isotopic fractionation. The modified LTOP model

developed by Smith and Barstad (2004) provides a promising method to estimate the precipitation field of a complex terrain. The model implies that the Patagonian Andes' intermittent rain can be represented by a mean precipitation rate. Furthermore, results from this study found that isotopes are set closer to the formation of hydrometeors than the formation of condensates. While the Smith and Evan's study (2007) was unsuccessful in finding a solution that included data from Stern and Blisniuk (2002), our model found a best-fit solution that created a good fit between the two data sets. The model estimated the variance for δD values as 61.1% and for $\delta^{18}O$ values as 48.1%. The hydrogen isotopes provided a better fit than the oxygen isotopes.

The development and results of this study have the potential to be applied to other orographic regions. In studies focused on determining paleoelevation estimates of mountains, this study can help determine the atmospheric dynamics that affect the relationship between stable isotopes from precipitation and mountain elevation.

Acknowledgements

I would like to thank Mark Brandon and David Auerbach who initially introduced me to this topic and guided me throughout my research. I would also like to give credit to Mark Brandon for his work in the compilation of the model code. I greatly appreciate the former work completed by Ron Smith, Idar Barstad and Alison Anders, from which this study was made possible.

References Cited

Crapper, G.D., 1958, A three-dimensional solution for waves in the lee of mountains: Journal of Fluid Mechanics, v. 6, p. 51-76.

Ellehoj, M.D., & al., 2013, Ice-vapor equilibrium fractionation factor of hydrogen and oxygen isotopes: Experimental investigations and implications for stable water isotope studies: Rapid Communications in Mass Spectrometry, v. 27, p. 2149-2158.

Forest, C.E., & al., 1999, Paleoaltimetry incorporating atmospheric physics and botanical estimates of paleoclimate: Geological Society American Bulletin, v. 111, p. 497-511.

Galewsky, J., 2009, Orographic precipitation isotopic ratios in stratified atmospheric flows: Implications for paleoelevation studies: Geology, v. 37, p. 791-794.

Garreaud, R., Lopez, P., Minvielle, M., and Rojas, M., 2013, Large-Scale Control on the Patagonian Climate: Journal of Climate, v. 26, p. 215-230.

Horita, J., and Wesolowski, D.J., 1994, Liquid-vapor fractionation of oxygen and hydrogen isotopes of water from the freezing to the critical temperature: Geochimica et Cosmochimica Acta, v. 58, p. 3425-3437.

Jiang, Q., and Smith, R.B., 2003, Cloud timescales and orographic precipitation: Journal of Atmospheric Science, v. 60, p. 1543-1559.

Nappo, C.J., 2002, An Introduction to Atmospheric Gravity Waves, Academic Press: p. 276.

Sahagian, D.L., and Maus, J.E., 1994, Basalt vesicularity as a measure of atmospheric pressure and paleoelevation: Nature, v. 372, p. 449-451.

Shatkay, H., 1995, The Fourier transform – A primer: Technical Report, Brown University, Providence, RI, USA.

Smith, R.B., 1979, The influence of mountains on the atmosphere: Advances in Geophysics, v. 21, p. 87-230.

Smith, R.B., 2006, Progress on the theory of orographic precipitation: Geological Society of America Special Paper 398, p. 1-6.

Smith, R.B., and Barstad, I., 2004, A linear theory of orographic precipitation: Journal of Atmospheric Sciences, v. 61, p. 1377-1391.

Smith, R.B., and Evans, J.P., 2007, Orographic precipitation and water vapor fractionation over the southern Andes: Journal of Hydrometeor, v. 8, p. 3-19.

Stern, L.A., and Blisniuk, P.M., 2002, Stable isotope composition of precipitation across the southern Patagonian Andes: Journal of Geophysical Research, v. 107, p. ACL3-1-ACL3-14.

Rowley, D.B., 2001, A new approach to stable isotope-based paleoaltimetry: implications for paleoaltimetry and paleohypsometry of the High Himalaya since the Late Miocene: Earth and Planetary Science Letters, v. 188, p. 253-268.

Rowley, D.B., and Garzione, C.N., 2007, Stable Isotope-Based Paleoaltimetry: Annual Review of Earth and Planetary Sciences, v. 35, p. 463-508.

Poage, M.A., and Chamberlain, C.P., 2001, Empirical Relationships between elevation and the stable isotope composition of precipitation and surface waters: considerations for studies of paleoelevation change: American Journal of Science, v. 301, p. 1-15.

Risi, C., Bony, S., and Vimeux, F., 2008, Influence of convective processes on the isotopic composition ($\delta^{18}O$ and δD) of precipitation and water vapor in the tropics: 2. Physical interpretation of the amount effect: Journal of Geophysical Research, v. 113, no. D19306

Appendix: MATLAB Code

A) quadrant_check.m : Finds the azimuth ranges and creates 1 km grid-spacing for the wind path of the sample at a given wind direction. It produces a display of the maximum and minimum azimuth values and a representation of the 1 km grid-spacing.

```
function quadrant_check
%% Create a 1 km lines that pass through each sample at a specific azimuth
clear all
close all
%%...Read the topography data
[x,y,h] = grdread('Patagonia_1kmGrid.nc');

%...find line through each sample point
% open and read the sample data from excel file
fid = fopen('Patagonian Andes Stern and Blisniuk 2005_xy.dat');
S1 = textscan(fid, '%f%f%f%f','treatAsEmpty',{'NAN','nan'}, ...
   'commentStyle','%');
fclose(fid);
fid = fopen('Patagonia Andes Smith and Evans 2007_xy.dat');
S2 = textscan(fid, '%f%f%f%f', ...
   'treatAsEmpty',{'NAN','nan'}, 'commentStyle','%');
fclose(fid);

%...Construct data into column vectors
xs = [S1{1}(:);S2{1}(:)];
ys = [S1{2}(:);S2{2}(:)];
%... The column vector source indicates the source of the data
source = [ones(size(S1{1}(:))); 2*ones(size(S2{2}(:)))];

%...initialize values
npoints = length(xs);
azimMin = 0;
azimMax = 180;
xMin = x(1);
xMax = x(end);
yMin = y(1);
yMax = y(end);
%% find the quadrant of each sample point

% find azimuth of line azim_13 and azim_24
azim_13 = atan2d(xMax-xMin,yMin-yMax);
azim_24 = atan2d(xMax-xMin,yMax-yMin);
% compare sample azimuths to diaganol azimuths, find limiting azimuths
for i = 1:npoints
   azim_1s = atan2d(xs(i)-xMin,ys(i)-yMax);
   azim_2s = atan2d(xs(i)-xMin,ys(i)-yMin);
```

```
   switch true
      case(azim_1s <= azim_13 && azim_2s >= azim_24)
         %...A quadrant, points max1 and min2 are limiting
         azimMaxPt = atan2d(xs(i)-xMin,ys(i)-yMax);
         azimMinPt = atan2d(xs(i)-xMin,ys(i)-yMin);
      case(azim_1s >= azim_13 && azim_2s >= azim_24)
         %...B quadrant, points max3 and min2 are limiting
         azimMaxPt = atan2d(xMax-xs(i),yMin-ys(i));
         azimMinPt = atan2d(xs(i)-xMin,ys(i)-yMin);
      case(azim_1s >= azim_13 && azim_2s <= azim_24)
         %...C quadrant, points max3 and min4 are limiting
         azimMaxPt = atan2d(xMax-xs(i),yMin-ys(i));
         azimMinPt = atan2d(xMax-xs(i),yMax-ys(i));
      case(azim_1s <= azim_13 && azim_2s <= azim_24)
         %...D quadrant, points max1 and min4 limiting
          azimMaxPt = atan2d(xs(i)-xMin,ys(i)-yMax);
          azimMinPt = atan2d(xMax-xs(i),yMax-ys(i));
   end
   if azimMinPt > azimMin
      azimMin = azimMinPt;
   end
   if azimMaxPt < azimMax
      azimMax = azimMaxPt;
   end
end
%% plot figures
figure(1)
subplot(1,2,1)
hold all
pcolor(x,y,h)
shading interp
cpmap = haxby;
cpmap = cmscale(h(:),cpmap,1);
colormap(cpmap);
for i = 1:npoints
   plot([xMin, xMax], ys(i) + [-(xs(i)-xMin), ...
      (xMax-xs(i))]/tand(azimMin), 'w-');
end
%... Plot Smith and Evans sample locations
plot(xs(source==1), ys(source==1), 'ro');
%... Plot Stern and Blisniuk  sample locations
plot(xs(source==2), ys(source==2), 'bo');
grid on
axis equal
axis([xMin,xMax,yMin,yMax]);
str = sprintf('  %s%5.1f  ','Minimum Azimuth = ',azimMin);
title(str)
```

```
xlabel('Easting (km)')
ylabel('Northing (km)')

% plotting maximum azimuth wind directions
subplot(1,2,2)
hold all
pcolor(x,y,h)
shading interp
cpmap = haxby;
cpmap = cmscale(h(:),cpmap,1);
colormap(cpmap);
for i = 1:npoints
   plot([xMin, xMax], ys(i) + [-(xs(i)-xMin), ...
      (xMax-xs(i))]/tand(azimMax), 'w-');
end
%... Plot Smith and Evans sample locations
plot(xs(source==1), ys(source==1), 'ro');
%... Plot Stern and Blisniuk  sample locations
plot(xs(source==2), ys(source==2), 'bo');
grid on
axis equal
axis([xMin,xMax,yMin,yMax]);
str = sprintf('  %s%5.1f  ','Maximum Azimuth = ',azimMax);
title(str)
xlabel('Easting (km)')
ylabel('Northing (km)')

%% create 1 km grid spacing
dP = 1; %1 km on azimuth line from each sample point
azim = azimMax;
for i = 1:1
   dx = dP*sind(azim);
   xPMin = xs(i) - dx*floor((xs(i)-xMin)/dx);
   xPMax = xs(i) + dx*floor((xMax-xs(i))/dx);
   xPi = (xPMin:dx:xPMax);
   yPi = (xPi-xs(i))*tand(azim)+ys(i);
   hPi = interp2(x,y,h,xPi,yPi);
   pPi = (xPi-xs(i))*sind(azim)+(yPi-ys(i))*cosd(azim);
end

% plotting maximum azimuth wind directions
figure(2)
hold all
pcolor(x,y,h)
shading interp
cpmap = haxby;
cpmap = cmscale(h(:),cpmap,1);
```

```
colormap(cpmap);
plot([xPi(1),xPi(end)],[yPi(1),yPi(end)], 'w-')
plot(xPi,yPi, 'wo')
% plot sample location
plot(xs(1), ys(1), 'ro');
grid on
axis equal
axis([xMin,xMax,yMin,yMax]);
str = sprintf('  %s%5.1f  ','Maximum Azimuth = ',azimMax);
title(str)
xlabel('Easting (km)')
ylabel('Northing (km)')
end
```

B) verticalWindSpeed.m: Finds the vertical wind speed for a given region. It produces a display of vertical wind speed, wind transect and a quiver plot.

```
function verticalWindSpeed
%% Calculate the steady vertical velocity field
%% initialize program
clear all
close all
clc
dbstop if error
%% user defined variables
gridFile = 'Patagonia_1kmGrid.nc';
mag = 30; %m/s
azimuth = 132; %degrees
Nm = 0.001; %s^-1
zContour = 100;
zLw = 0;
zHi = 10000;
zD = 1000;
%% Start calculation
% define windspeed
u = mag*sind(azimuth);
v = mag*cosd(azimuth);
%%...Read the topography data
[x,y,h] = grdread(gridFile);
x = x*1e3;
y = y*1e3;
nX = length(x);
nY = length(y);
dX = abs(x(2)-x(1));
dY = abs(y(2)-y(1));
% Calculate wavenumber vectors for x and y
```

```
iXMostNeg = ceil(nX/2)+1;
iYMostNeg = ceil(nY/2)+1;
kX = (0:nX-1)/nX;
kX(iXMostNeg:nX)=kX(iXMostNeg:nX)-1;
kX = 2*pi*kX/dX;
kY = (0:nY-1)/nY;
kY(iYMostNeg:nY)=kY(iYMostNeg:nY)-1;
kY = 2*pi*kY/dY;
[KX,KY] = meshgrid(kX,kY);
% Calculate fourier transform
H = fft2(h);
sigma = u*KX+v*KY;
sigma(sigma==0)=1e-7;
iSigma = abs(sigma) < 1e-7;
sigma(iSigma) = sign(sigma(iSigma))*1e-7;
m = sqrt(((Nm./sigma).^2 -1).*(KX.^2+KY.^2));
W = 1i*sigma.*exp(1i*m.*zContour).*H;
w = real(ifft2(W));
wContour = real(ifft2(W));
% Calculate quiver plot
nStep = 25;
nWrows = floor((zHi-zLw)/zD)+1;
xQuiver = x(1:nStep:nX);
nXQuiver = length(xQuiver);
zQuiver = (0:nWrows-1)*zD+zLw;
UQuiver = ones(nWrows,nXQuiver)*u;
WQuiver = zeros(nWrows,nXQuiver);
for i = 1:nWrows
   W = 1i*sigma.*exp(1i*m.*zQuiver(i)).*H;
   w = real(ifft2(W));
   WQuiver(i,:) = w(ceil(nY/2),1:nStep:nX);
end
%% plot figures
figure(1)
pcolor(x*1e-3,y*1e-3,h)
shading interp
cpmap = haxby;
cpmap = cmapscale(h,cpmap,1);
colormap(cpmap);
grid on
axis equal tight
box on
hFig = colorbar;
ylabel(hFig,'Elevation (m)')
title('Topography')
xlabel('Easting (km)')
ylabel('Northing (km)')
```

```
% plot vertical wind speed at 1 km
figure(2)
pcolor(x*1e-3,y*1e-3,wContour)
shading interp
cpmap = coolwarm;
cpmap = cmscale(wContour(:),cpmap,.5);
colormap(cpmap);
grid on
axis equal tight
box on
hFig = colorbar;
ylabel(hFig,'Vertical Wind Speed (m/s)')
title('Vertical Wind Speed')
xlabel('Easting (km)')
ylabel('Northing (km)')

figure(3)
plot(x*1e-3,w(ceil(nY/2),:));
title('Vertical Wind Speed Along Center Line')
xlabel('Easting (km)')
ylabel('w (m/s)')

figure(4)
hold on
axis([-5*1e5 5*1e5 0 12000])
q = quiver(xQuiver,zQuiver,UQuiver*500,WQuiver*500,0);
adjust_quiver_arrowhead_size(q,.2);
plot(x,h,'-k','Linewidth',3)
title('Quiver Plot')
ylabel('Elevation (m)')
xlabel('Easting (m)')
end
```

C) ItopWithIsotopes.m: Estimates the stable isotopic values for a given elevation with the inclusion of 8 parameters. It produces a display of topography, mean precipitation height, mean precipitation rate, mean precipitation temperature, and mean surface temperature.

```
function ItopWithIsotopes
%% Calculate the steady precipitation-rate field and isotope fields

%% Initialize system
clear all
close all
clc
dbstop if error
```

```
%% User-defined variables
gridFile = 'Patagonia_1kmGrid.nc';
U = 30;            % horizontal wind speed (m/s)
azimuth = 132;      % horizontal wind direction (degrees from +y towards +x)
tauC = 725;         % condensation time (s)
tauF = 725;         % fall-out time (s)
T0 = 274;           % sea-level temperature (K)
Nm = 0.001;         % moist Brunt-Vaisala frequency (cycles/s)
latitude = 45;      % average latitude for Coriolis frequency (deg)
deltaH20 = -52.8e-3; % estimate for initial delta D (per unity)
deltaO180 = -5.3e-3; % estimate for initial delta O18 (per unity)

%... Coriolis frequency (rad/s)
f = 2*7.2921e-5*sind(latitude);
%... Set to zero when mountain width < ~200 km
%f = 0;
%% Constants
TK2C = 273.15;     % conversion from Kelvin to Celcius

%% Start calculation
% Calculate atmospheric parameters
[gammaCap,gamma,Hw,rhoS0] = moistAdiabat(Nm,T0);
%... Define windspeed
u = U*sind(azimuth);
v = U*cosd(azimuth);
%%...Read topography data
[x,y,h] = grdread(gridFile);
x=x*1e3;
y=y*1e3;
[X, Y] = meshgrid(x,y);
xMin = x(1);
xMax = x(end);
yMin = y(1);
yMax = y(end);
dX = abs(x(2)-x(1));
dY = abs(y(2)-y(1));
nX = length(x);
nY = length(y);
nXPad = round(1.2*nX);
nYPad = round(1.2*nY);

%... Calculate wavenumber vectors for x and y (rad/m)
iXMostNeg = ceil(nXPad/2)+1;
iYMostNeg = ceil(nYPad/2)+1;
kX = (0:nXPad-1)/nXPad;
kX(iXMostNeg:nXPad)=kX(iXMostNeg:nXPad)-1;
kX = 2*pi*kX/dX;
```

```
kY = (0:nYPad-1)/nYPad;
kY(iYMostNeg:nYPad)=kY(iYMostNeg:nYPad)-1;
kY = 2*pi*kY/dY;
[KX,KY] = meshgrid(kX,kY);
%... Calculate fourier transform
hHat = fft2(h,nYPad,nXPad);
%... Calculate intrinsic frequencies (rad/s)
sigma = u*KX + v*KY;
%... Calculate denominator for m equation, and modify to
% avoid division-by-zero errors.
denom = sigma.^2 - f^2;
denom(denom==0) = eps;
%... Calculate vertical wave numbers
m = sqrt((((2*pi*Nm)^2./denom) -1).*(KX.^2 + KY.^2));
%... Calculate precipitation rate
rpHat = (gammaCap.*1i.*sigma.*hHat./gamma) ...
   ./((1 - 1i.*m*Hw).*(1+1i.*sigma.*tauC).*(1+1i.*sigma.*tauF));
rp = real(ifft2(rpHat));
rp = rp(1:nY,1:nX);
rp(rp<=0) = 0;

%... Calculate mean precipitation height
zpHat = (gammaCap*Hw.*1i.*sigma.*hHat./gamma) ...
   ./((1 - 1i.*m*Hw).^2.*(1+1i.*sigma.*tauC).*(1+1i.*sigma.*tauF));
zp = real(ifft2(zpHat));
zp = zp(1:nY,1:nX);
zp = abs(zp./rp);
%... zp is restricted to values less than 3*Hw
zp(zp>3*Hw) = 3*Hw;

%... Mean temperature at source
Tc = T0 - gammaCap*(zp + h);

... Mean temperature at surface
Ts = T0 - gammaCap*h;

%...Open and read the sample data from excel file
fid = fopen('Patagonian Andes Stern and Blisniuk 2005_xy.dat');
S1 = textscan(fid, '%f%f%f%f','treatAsEmpty',{'NAN','nan'}, ...
   'commentStyle','%');
fclose(fid);
fid = fopen('Patagonia Andes Smith and Evans 2007_xy.dat');
S2 = textscan(fid, '%f%f%f%f', ...
   'treatAsEmpty',{'NAN','nan'}, 'commentStyle','%');
fclose(fid);
%...Construct data into column vectors
xSample = [S1{1}(:);S2{1}(:)]*1e3;
```

```
ySample = [S1{2}(:);S2{2}(:)]*1e3;
deltaO18Sample = [S1{3}(:);S2{3}(:)]*1e-3;
deltaH2Sample = [S1{4}(:);S2{4}(:)]*1e-3;

%... Calculate precipitation rate at sample locations
nSample = length(xSample);
dS = (dX + dY)/2;
pSample = zeros(nSample,1);
hSample = zeros(nSample,1);
rhoSrSample = zeros(nSample,1);
deltaH2_TcPred = zeros(nSample,1);
deltaO18_TcPred = zeros(nSample,1);
deltaH2_TsPred = zeros(nSample,1);
deltaO18_TsPred = zeros(nSample,1);
%... Iterate over the samples
for i = 1:nSample
   %... Find s coordinate for most upstream point along wind path
   % passing through the sample location. Wind is assumed to flow
   % through the xMin side of the topographic grid.
   sMinPath = (xMin - xSample(i))*sqrt(1+cosd(azimuth)^2);
   sMinPath = dS*ceil(sMinPath/dS);
   %... Calculate x,y coordinates for points from s = sMinPath
   % to s = 0, which marks the sample location along the wind path.
   xPath = xSample(i) + (sMinPath:dS:0)*sind(azimuth);
   yPath = ySample(i) + (sMinPath:dS:0)*cosd(azimuth);
   %... Interpolate topographic grid to get elevations along wind path
   hPath = interp2(X,Y,h,xPath,yPath);
   hSample(i) = hPath(end);
   %... Interpolate rp grid to get relative precipation values along wind path
   rpPath = interp2(X,Y,rp,xPath,yPath);
   %... Calculate reduced water-varpor density at land surface along wind path
   rhoSrPath = rhoS0.*exp(-cumtrapz(rpPath)*dS/(Hw*U));
   rhoSrSample(i) = rhoSrPath(end);
   %... Calculate precipitation rate along wind path
   pPath = rpPath.*rhoSrPath;
   pSample(i) = pPath(end);
   %... Calculate mean condensation temperature along wind path
   TcPath = interp2(X,Y,Tc,xPath,yPath);
   %... Hydrogen isotopic composition for CE case
   alpha = hydrogenFractionation(TcPath);
   deltaH2_TcPred(i) = ...
      log(alpha(end)/alpha(1)) + deltaH20 - trapz((alpha-1).*rpPath).*dS./(Hw*U);
   %... Oxygen isotopic composition for CE case
   alpha = oxygenFractionation(TcPath);
   deltaO18_TcPred(i) = ...
      log(alpha(end)/alpha(1)) + deltaO180 - trapz((alpha-1).*rpPath).*dS./(Hw*U);
   %... Calculate land-surface temperature along wind path
```

```
    TsPath = interp2(X,Y,Ts,xPath,yPath);
    %... Hydrogen isotopic composition for PE case
    alpha = hydrogenFractionation(TsPath);
    deltaH2_TsPred(i) = ...
        log(alpha(end)/alpha(1)) + deltaH20 - trapz((alpha-1).*rpPath).*dS./(Hw*U);
    %... Oxygen isotopic composition for PE case
    alpha = oxygenFractionation(TsPath);
    deltaO18_TsPred(i) = ...
        log(alpha(end)/alpha(1)) + deltaO180 - trapz((alpha-1).*rpPath).*dS./(Hw*U);
end
%... Calculate standard deviation of the residuals for the observed
% versus predicted stable isotope measurements
n = sum(~isnan(deltaH2Sample));
sd_deltaH2_Tc = nanstd(deltaH2Sample - deltaH2_TcPred, 1) * sqrt(n/(n-8));
n = sum(~isnan(deltaO18Sample));
sd_deltaO18_Tc = nanstd(deltaO18Sample - deltaO18_TcPred, 1) * sqrt(n/(n-8));
n = sum(~isnan(deltaH2Sample));
sd_deltaH2_Ts = nanstd(deltaH2Sample - deltaH2_TsPred, 1) * sqrt(n/(n-8));
n = sum(~isnan(deltaO18Sample));
sd_deltaO18_Ts = nanstd(deltaO18Sample - deltaO18_TsPred, 1) * sqrt(n/(n-8));

%% Report results
%... Report characteristic height for water vapor distribution
fprintf('Characteristic height for water vapor, Hw (m) = %5.0f\n', Hw);
%... Calculate regional mean for precipitation height
iFinite = ~isnan(zp);
weights = rp(iFinite)./sum(rp(iFinite));
zpRegionalMean = sum(weights.*zp(iFinite));
fprintf('Regional mean for precipitation height (m): %5.0f\n', zpRegionalMean);
%... Standard deivation of the residuals
fprintf('====== STANDARD DEVIATION OF THE RESIDUALS =====\n')
fprintf('CE case, delta 2H (per mil): %g\n', sd_deltaH2_Tc*1e3)
fprintf('CE case, delta 18O (per mil): %g\n', sd_deltaO18_Tc*1e3)
fprintf('PE case, delta 2H (per mil): %g\n', sd_deltaH2_Ts*1e3)
fprintf('PE case, delta 18O (per mil): %g\n', sd_deltaO18_Ts*1e3)

%% Plot figures
%... Plot topography
figure(1)
pcolor(x*1e-3,y*1e-3,h)
shading interp
cpmap = haxby;
cpmap = cmapscale(h,cpmap,1);
colormap(cpmap);
axis equal tight
hFig = colorbar;
ylabel(hFig,'  Elevation (m)  ')
```

```
title('  Topography')
xlabel('  Easting (km)  ')
ylabel('  Northing (km) ')

%... Plot relative precipitation rate
figure(2)
pcolor(x*1e-3,y*1e-3,rp*1e3)
shading interp
cpmap = coolwarm;
cpmap = cmapscale(rp*1e3,cpmap,0.5);
colormap(cpmap);
axis equal tight
hFig = colorbar;
ylabel(hFig,'  Relative Precipitation Rate  ')
title('  Relative Precipitation Rate   ')
xlabel('  Easting (km)  ')
ylabel('  Northing (km)  ')

%... Plot mean height for precipitation
figure(3)
pcolor(x*1e-3,y*1e-3, log10(zp*1e-3))
shading interp
cpmap = coolwarm;
cpmap = cmapscale(log10(zp*1e-3),cpmap,0.25);
colormap(cpmap);
axis equal tight
hFig = colorbar;
ylabel(hFig,'  Height (log10 km)  ')
title('  Mean Precipitation Height  ');
xlabel('  Easting (km)  ')
ylabel('  Northing (km)  ')

%... Plot mean temperature for precipitation
figure(4)
T = Tc-TK2C;
T(T<-TK2C) = -TK2C;
pcolor(x*1e-3,y*1e-3, T)
shading interp
cpmap = coolwarm;
cpmap = cmapscale(T,cpmap,1,0);
colormap(cpmap);
axis equal tight

hFig = colorbar;
ylabel(hFig,'  Temperature (C)  ')
title('  Mean Precipitation Temperature  ');
xlabel('  Easting (km)  ')
```

```
ylabel('  Northing (km)  ')

%... Plot land surface temperature
figure(5)
T = Ts-TK2C;
pcolor(x*1e-3,y*1e-3, T)
shading interp
cpmap = coolwarm;
cpmap = cmapscale(T,cpmap,1,0);
colormap(cpmap);
axis equal tight
hFig = colorbar;
ylabel(hFig,'  Temperature (C)  ')
title('  Land Surface Temperature  ');
xlabel('  Easting (km)  ')
ylabel('  Northing (km)  ')

%... Plot mean precipitation height
figure(6)
plot(log10(rp*1e3),log10(zp.*1e-3),'.k')
xlabel('  Relative Precipitation Rate (log10)  ')
ylabel('  Mean Preciptation Height (log 10 km)  ')

%... Plot predicted vs observed isotope values
xMin = min([deltaH2Sample(:);deltaO18Sample(:);deltaH20;deltaO180]*1e3);
xMax = max([deltaH2Sample(:);deltaO18Sample(:);deltaH20;deltaO180]*1e3);
yMin = min([deltaH2_TcPred(:);deltaO18_TcPred(:); ...
   deltaH2_TsPred(:);deltaO18_TsPred(:);deltaH20;deltaO180]*1e3);
yMax = max([deltaH2_TcPred(:);deltaO18_TcPred(:); ...
   deltaH2_TsPred(:);deltaO18_TsPred(:);deltaH20;deltaO180]*1e3);
xMin = floor(min([xMin,yMin]));
xMax = ceil(max([xMax,yMax]));

subplot(1,2,1) %... CE case
hold on
%... Plot 1:1 reference line
plot([xMin,xMax],[xMin,xMax],'-','Color',[0.4 0.4 0.4],'LineWidth',3)
%... Plot isotope data
plot(deltaH2Sample*1e3, deltaH2_TcPred*1e3,'ob')
plot(deltaO18Sample*1e3, deltaO18_TcPred*1e3, 'or')
%... Plot initial values for isotopes
plot(deltaH20*1e3, deltaH20*1e3,'sb','MarkerSize',24)
plot(deltaO180*1e3, deltaO180*1e3, 'sr','MarkerSize',24)
axis square
xlim([xMin,xMax]);
ylim([xMin,xMax]);
title('Stable Isotopes for CE Case')
```

```
xlabel('Sample (per mil)')
ylabel('Calculated (per mil)')

subplot(1,2,2) %... PE case
hold on
%... Plot 1:1 reference line
plot([xMin,xMax],[xMin,xMax],'-','Color',[0.4 0.4 0.4],'LineWidth',3)
%... Plot isotope data
plot(deltaH2Sample*1e3, deltaH2_TsPred*1e3,'ob')
plot(deltaO18Sample*1e3, deltaO18_TsPred*1e3, 'or')
%... Plot initial values for isotopes
plot(deltaH20*1e3, deltaH20*1e3,'sb','MarkerSize',24)
plot(deltaO180*1e3, deltaO180*1e3, 'sr','MarkerSize',24)
axis square
xlim([xMin,xMax]);
ylim([xMin,xMax]);
title('Stable Isotopes for PE Case')
xlabel('Sample (per mil)')
ylabel('Calculated (per mil)')
end
```